Hydrogen storage properties of the refractory Ti–V–Zr–Nb–Ta multi-principal element alloy

Jorge Montero, Gustav Ek, Laetitia Laversenne, Vivian Nassif, Guilherme Zepon, Martin Sahlberg, Claudia Zlotea

Hydrogen storage properties of the refractory Ti-V-Zr-Nb-Ta multi-principal element alloy

Jorge Montero[1], Gustav Ek[2], Laetitia Laversenne[3], Vivian Nassif[3], Guilherme Zepon[4], Martin Sahlberg[2], Claudia Zlotea[1*]

[1]*Univ Paris Est Créteil, CNRS, ICMPE, UMR 7182, 2 rue Henri Dunant, 94320 Thiais, France*

[2]*Department of Chemistry, Uppsala University, Box 523, SE-75120 Uppsala, Sweden*

[3]*University Grenoble Alpes, CNRS, Grenoble INP, Institut Néel, 38000 Grenoble, France*

[4]*Department of Materials Engineering, Federal University of São Carlos, Rod. Washington Luis, km 235, CEP: 13565-905, São Carlos-SP, Brazil*

* Corresponding author: claudia.zlotea@icmpe.cnrs.fr

Abstract

A new quinary multi-principal element alloy $Ti_{0.30}V_{0.25}Zr_{0.10}Nb_{0.25}Ta_{0.10}$ was prepared by high temperature melting technique and the physicochemical as well as hydrogen sorption properties have been determined. The as-cast alloy crystallizes into a single-phase *bcc* lattice and can very quickly absorb hydrogen at room temperature forming a *fcc* hydride phase with capacity of 2 H/*M* (2.5 wt.%). The absorption/desorption of hydrogen is reversible and occurs within one step, as proven by *in situ* neutron diffraction for the desorption reaction. The capacity is slightly fading during the first 10 cycles and then stabilizes at around 2.2 wt.% for the next 10 cycles.

Key words: Multi-principal element alloys, high entropy alloys, hydrogen absorption and desorption, in situ neutron diffraction, cycling stability

1. Introduction

Hydrogen is considered as an interesting alternative to reduce fossil fuel consumption and mitigate the environmental impact caused by fuel combustion. Hydrogen possesses the highest energy density compared to other fuels on the market and its combustion is pollution-free. However, one of the main challenges of using hydrogen as a clean energy carrier is its safe storage and transportation.[1] One promising method is to store hydrogen in metals/alloys/intermetallics, known as metal hydrides, as they can safely store hydrogen in the solid-state form. An ideal metal/alloy must fulfill the following criteria: high hydrogen storage capacity, reversibility of absorption and desorption at reasonable pressure and temperature conditions, fast kinetics of both processes and good cycle life without capacity degradation or phase segregation. Also, it must be as lightweight as possible, cost-effective in large scale amounts and free of risk for the users of the storing device. Different metal/alloys have been investigated to store hydrogen, for example, Mg-based alloys is one of the most documented class of materials. [2]

One recent approach is to use multi-principal element alloys (MPEA) which are mixtures of four or more elements in near equimolar conditions adopting simple crystalline structures (body centered cubic: *bcc*, face centered cubic: *fcc*, hexagonal compact: *hcp*), also known as high entropy alloys (HEA).[3,4] MPEAs have been widely investigated for potential industrial applications due to their interesting and outstanding mechanical properties.[5] These alloys are characterized by a significant degree of lattice distortion as they are made from many elements with different atomic radius; as a consequence, they may develop large interstitial sites that can make these alloys promising candidates for solid-state hydrogen storage. Despite this

interesting feature and the massive number of possible new compositions, limited studies on hydrogen sorption properties have been reported previously.[6–13] Among all MPEAs, our interest lays in *bcc* alloys containing refractory elements since these individual metals can absorb large amount of hydrogen forming hydride with a maximum capacity of 2 H/*M*.[14] Our first study on the *bcc* TiVZrNbHf composition exceeded this limit and reported a capacity of 2.5 H/*M*, which made the refractory MPEAs a very promising class of materials for solid-state hydrogen storage.[7] However, one of the main drawbacks of these alloys is the disproportionation during hydrogen absorption/desorption and the poor cycle life stability, which is a parameter very scarcely reported. Many *bcc* refractory MPEAs have been reported to segregate into several *bcc* phases during hydrogen absorption/desorption cycling [6,11] or to oxidize during high temperature desorption (~ 973 K) [13]. These behaviors are the main responsible for the capacity fading during cycling.[12]

In the present study we report the synthesis by arc melting, the hydrogen absorption/desorption properties and the cycling stability of the new refractory MPEA $Ti_{0.30}V_{0.25}Zr_{0.10}Nb_{0.25}Ta_{0.10}$. This composition was chosen with respect to our recently published quaternary alloy $Ti_{0.325}V_{0.275}Zr_{0.125}Nb_{0.275}$ [15]. The aim is to study the effect of 10% addition of Ta into the initial quaternary composition on the structural, hydrogen sorption and cyclability properties.

2. Materials and Methods

$Ti_{0.30}V_{0.25}Zr_{0.10}Nb_{0.25}Ta_{0.10}$ (77.55 g/mol) was synthesized by high-temperature arc melting starting from bulk pieces of Ti (Alfa Aesar, 99.99%), Zr (Neyco, 99.95%), Nb (Alfa Aesar, 99.95%), metal sheets of V (Alfa Aesar, 99.7%) and Ta (Alfa Aesar, 99.76%). The alloy was melted under Ar atmosphere, re-melted and turned over 15 times to improve the homogeneity. The alloy was crushed and hand-milled in the form of coarse powder for further characterization.

Pressure-compositions isotherms (PCI) and kinetics of absorption were measured in an automated Sievert apparatus PCTPro-2000 (250 bar pressure gauge) or a manual home-made volumetric rig (100 bar pressure gauge) using a stainless-steel sample holder with metal gaskets. A resistance furnace was used to control the temperature during the absorption/desorption measurements. Before hydrogenation, the alloy was cut into small pieces and submitted to an activation treatment at 613 K for 2 hours under dynamic vacuum, 10^{-3} mbar of base pressure. The hydrogen absorption/desorption cyclability was tested on a manual volumetric Sievert apparatus at room temperature, thermostated by a water bath at 298 K. The absorption conditions were an initial pressure of H_2 (grade N6) of ~ 30 bar and 1 hour of equilibrium time. The hydrogen desorption was done by heating the sample to 683 K for 5 hours under dynamic secondary vacuum, typically 10^{-5} mbar.

The structural analysis was carried out by powder X-ray diffraction (XRD), before and after the hydrogenation and after 20 absorption/desorption cycles by the help of a D8 Advance Bruker diffractometer with Cu K_α wavelength and Bragg-Brentano geometry.

In-situ neutron powder diffraction experiments were performed during deuterium desorption at the Institute Laue-Langevin Grenoble, France, on the D1B beamline. The powder sample was

placed inside a silica tube sample holder under a dynamic secondary vacuum environment. A resistive furnace was used to heat the sample with a heating ramp of 1 K/min. The diffraction patterns were collected at the wavelength λ = 1.28 Å using a step of 0.1 ° from 0.77° to 128.77° 2Θ. The pressure of evolved gas was continuously recorded during the desorption experiment with the help of a vacuum gauge.

The crystalline structure of the alloy, hydride and deuteride phases were analyzed using the Rietveld method implemented in the Fullprof software on both XRD and neutron diffraction patterns.[16]

Scanning electron microscopy (SEM) was used to analyze the microstructure of the alloy after the first and twentieth hydrogen absorption/desorption cycle on a Zeiss Merlin microscope complemented with energy dispersive spectroscopy (EDS) from Oxford Instruments (AZtec EDS Advanced) to determine the chemical compositions.

The desorption properties were characterized by thermo-desorption spectroscopy (TDS) and differential scanning calorimetry (DSC). In TDS, the instrument is a home-made apparatus coupled to a mass spectrometer, as described in a previous work [17]. Around 10 mg of the sample was loaded into an aluminum crucible inside a glovebox with Ar atmosphere. The temperature was controlled by a resistance furnace with a heating ramp of 1 K/min up to around 650 K and a secondary pump was employed to reach a vacuum pressure of 10^{-6} mbar. The H_2/D_2 partial pressures were monitored with a quadruple mass spectrometer during the constant heating ramp. The DSC was measured on Netzsch STA 449 C instrument and coupled to a quadruple mass spectrometer (QMS). A heating ramp was set to 10 K/min up to 873 K and Ar flow was used as gas carrier.

3. Results and discussions

3.1 Synthesis of the $Ti_{0.30}V_{0.25}Zr_{0.10}Nb_{0.25}Ta_{0.10}$ pristine alloy

The MPEA with the following composition $Ti_{0.30}V_{0.25}Zr_{0.10}Nb_{0.25}Ta_{0.10}$ was synthesized by arc melting technique. The valence electron concentration (*VEC*) for this composition is 4.6 and the lattice distortion, δ, as described by Ye *et al*. [18] is determined to be 5.5 %. For this calculation, the atomic radius of each element was taken from reference.[19]

The alloy was characterized by powder XRD (Figure 1) and crystallizes in a single-phase *bcc* structure with the $Im\bar{3}m$ space group and the lattice parameter *a* = 3.263(1) Å, as determined by Rietveld analysis. This value is very close to the lattice parameter of 3.261(1) Å for the quaternary alloy $Ti_{0.325}V_{0.275}Zr_{0.125}Nb_{0.275}$, reported recently.[15] This is not surprising since Ta possesses an atomic radius (1.43 pm) very close to the ones of Ti (1.45 pm) and Nb (1.43 pm).

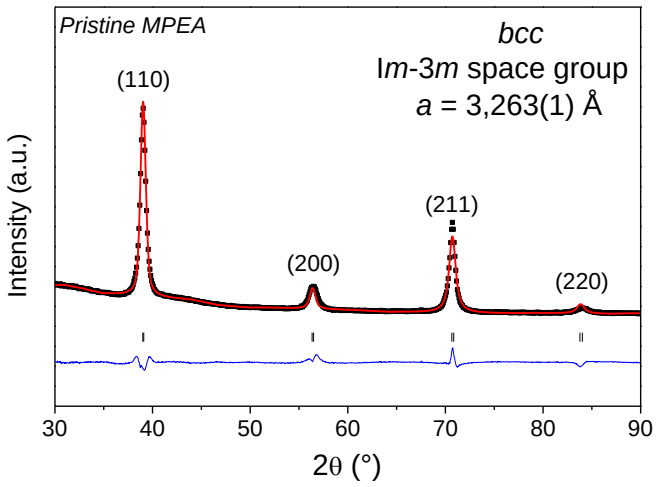

Figure 1. XRD of the as-cast MPEA $Ti_{0.30}V_{0.25}Zr_{0.10}Nb_{0.25}Ta_{0.10}$ together with the corresponding Rietveld refinement. ($\lambda_{Cu\ K\text{-}\alpha}$ = 1.5406 Å)

Hence, the classical metallurgical method of arc melting fusion was successfully applied to prepare single-phase *bcc* $Ti_{0.30}V_{0.25}Zr_{0.10}Nb_{0.25}Ta_{0.10}$ alloy.

3.2 Hydrogen absorption of $Ti_{0.30}V_{0.25}Zr_{0.10}Nb_{0.25}Ta_{0.10}$

Before measuring the hydrogen storage capacity of the alloy, a short activation step was performed in order to promote hydrogen uptake and enhance the kinetics of absorption. Therefore, a heat treatment at 613 K for 2 hours was performed in a continuous vacuum environment.

The alloy has a maximum hydrogen absorption capacity of 2.0 H/*M* (2.5 wt.%), as proved by the kinetics measurement recorded under 33 bar of hydrogen pressure at 373 K (Figure 2A). The absorption is very fast and within a single-step reaction reaching 98 % of the full capacity in only 2 minutes. The XRD of the hydride phase (inset of Figure 2A) shows a single-phase material with a structure that can be described by either *bct* (*I4/mmm* space group) or *fcc* (*Fm-3m* space group) lattices. The confidence factors of Rietveld refinements for both structures are very similar (table SI1 for both XRD and neutron diffraction data). The *bct* structure can be described as a slightly distorted *fcc* lattice and, MPEAs are characterized by owning an important degree of lattice distortion. This has been observed in other hydrides of MPEAs based on refractory elements.[15,20]

After the first absorption, the sample was subsequently desorbed by heating at 673 K under dynamic secondary vacuum for 5 hours. After cooling to room temperature, a PCI curve was measured at 298 K (Figure 2B) on the second hydrogenation cycle. The plot shows a single equilibrium pressure plateau below 1 bar, similar to other refractory *bcc* MPEAs, with a single-phase transition from *bcc* → *bct/fcc* upon hydrogenation.[7,15,20] The equilibrium pressure is within the range of milibars or below and cannot be accurately determined since these values are in the reading limit of our high pressure gauge. The alloy has a maximum hydrogen capacity

of 1.73 H/*M* (2.2 wt.%), which is slightly less than 2.0 H/*M* initially observed. The decay of the capacity during cycling will be further discussed in a dedicated section.

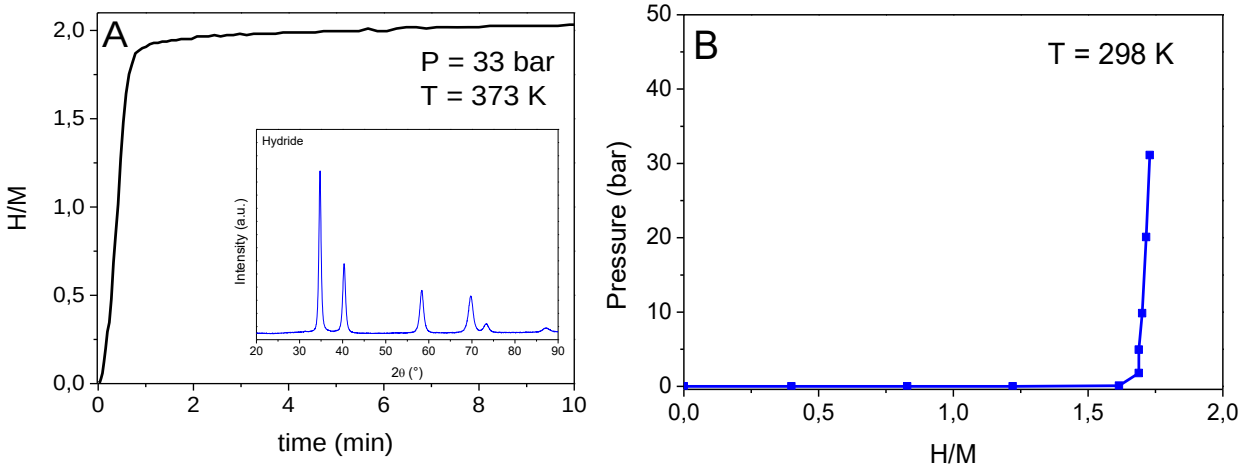

Figure 2. A: First cycle absorption kinetics for $Ti_{0.30}V_{0.25}Zr_{0.10}Nb_{0.25}Ta_{0.10}$ at 373 K (inset: XRD of the hydride phase with $\lambda_{Cu\ K\text{-}\alpha}$ = 1.5406 Å). B: Pressure-Composition-Isotherm at 298 K for the second absorption cycle.

This behavior towards hydrogen is in agreement with our previous findings for the quaternary alloy $Ti_{0.325}V_{0.275}Zr_{0.125}Nb_{0.275}$, which also shows a single-step transition during hydrogen absorption but with a slightly smaller maximum capacity of 1.75 H/*M*.[15]

To further characterize the crystalline structure of the hydride phase, neutron diffraction experiments have been performed using deuterium instead of hydrogen. The deuteride phase with D/*M* = 2 was prepared by exposing the pristine alloy to 33 bar of deuterium at 373 K for 1 h, similarly to the pressure and temperature conditions used for the kinetic curve in Figure 2A. The neutron diffraction pattern and related Rietveld analysis are displayed in Figure 3 and similar conclusion as XRD analysis can be drawn: the crystalline structure can be described by

either *bct* or *fcc* lattices (Table SI1 and Figure SI1). The deuterium atoms have been localized within the tetragonal interstitial sites of the *bct* (*I4/mmm* space group) or the *fcc* ($Fm\bar{3}m$ space group) lattices.

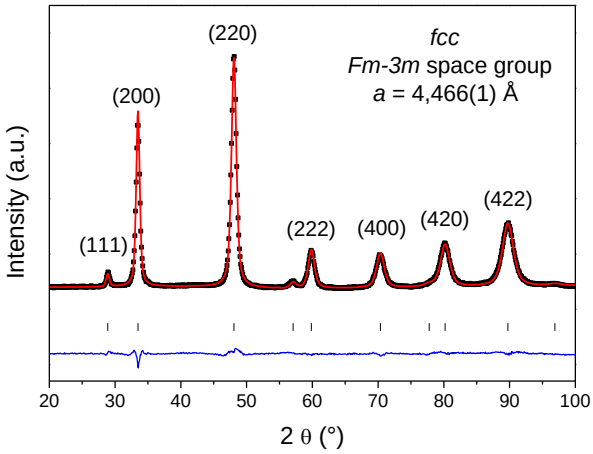

Figure 3. *Ex-situ* neutron diffraction of $Ti_{0.30}V_{0.25}Zr_{0.10}Nb_{0.25}Ta_{0.10}D_2$ and corresponding Rietveld refinement based on *fcc* lattice (λ = 1.28 Å).

In summary, the $Ti_{0.30}V_{0.25}Zr_{0.10}Nb_{0.25}Ta_{0.10}$ MPEA rapidly absorbs hydrogen/deuterium in the temperature region 298-373 K within a single step reaction and forms a *fcc/bct* hydride/deuteride phase with a maximum capacity of 2 H(D)/*M*. This value is surpassing the maximum hydrogen storage capacity of 1.75 H/*M* obtained for our previously reported quaternary $Ti_{0.325}V_{0.275}Zr_{0.125}Nb_{0.275}$ MPEA prepared by similar method.[15] This suggests that the addition of only 10% of Ta within the $Ti_{0.325}V_{0.275}Zr_{0.125}Nb_{0.275}$ alloy is beneficial for the increase of the maximum storage capacity, as expressed in H/*M*.

3.3 Hydrogen desorption from $Ti_{0.30}V_{0.25}Zr_{0.10}Nb_{0.25}Ta_{0.10}$ hydride/deuteride

Three experimental techniques were used to characterize the desorption properties of the hydride/deuteride phases: two thermal analysis methods (TDS and DSC coupled with mass spectrometry) and one structural technique (*in situ* neutron diffraction).

The TDS profile in Figure 4 (heating rate 1 K/min) shows two distinct broad peaks with the onset temperature at ~ 400 K and the maximum desorption rates at 430 K and 535 K. It is worth to compare this result with our previous finding for the quaternary $Ti_{0.325}V_{0.275}Zr_{0.125}Nb_{0.275}$ alloy prepared by similar method.[15] The quaternary alloy possesses an onset temperature of 500 K, which is around 100 K more than the Ta-containing alloy, and two maxima at 525 K and 600 K.

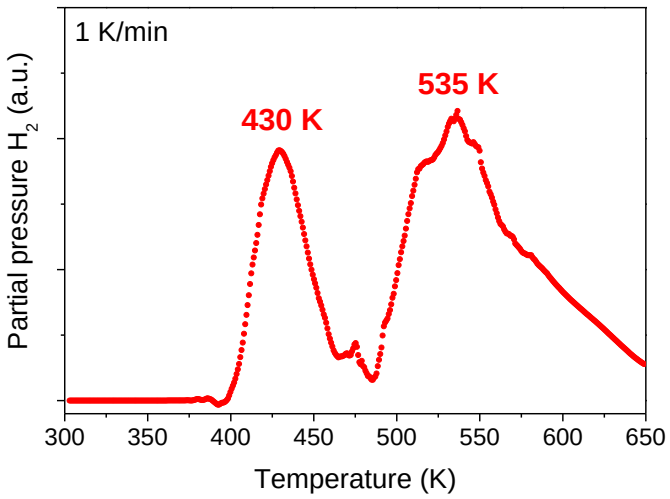

Figure 4. TDS desorption profile for $Ti_{0.30}V_{0.25}Zr_{0.10}Nb_{0.25}Ta_{0.10}H_2$ recorded as a function of temperature, using a heating ramp of 1 K/min under secondary vacuum.

The second thermo-analysis characterization was carried out by differential scanning calorimetry (DSC) with a temperature ramp of 10 K/min (Figure 5). The hydrogen QMS signal (dotted line) matches perfectly with the endothermic events (continuous line) suggesting two stages hydrogen desorption reaction.

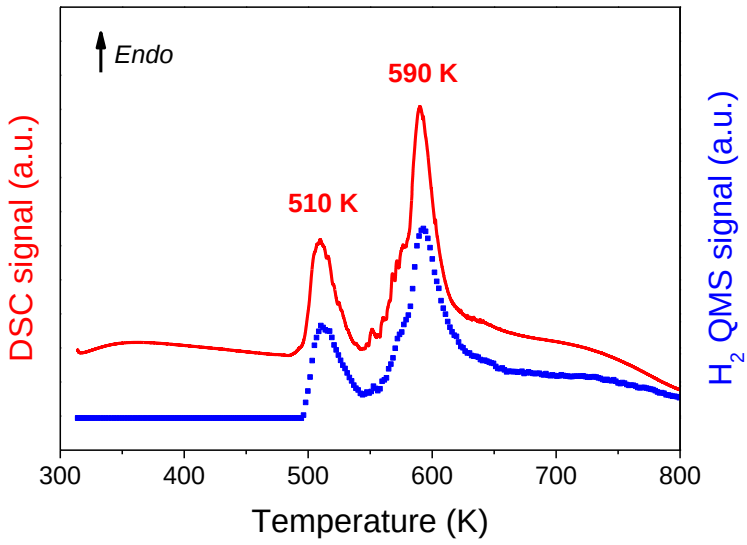

Figure 5. DSC-QMS signals during hydrogen desorption from $Ti_{0.30}V_{0.25}Zr_{0.10}Nb_{0.25}Ta_{0.10}H_2$ with a temperature ramp of 10 K/min (in Ar flow).

It is important to notice that the two main endothermic events are similar to those measured by TDS but shifted towards higher temperatures. This difference is not surprising since the heating ramp for DSC is much faster (10 K/min) as compared to TDS (1 K/min). It is well known that the maximum of the temperature peaks drifts to higher temperatures for higher heating rates. Another possible explanation is based on the intrinsic differences between TDS and DSC instruments where the measurement principles and environments are dissimilar.

The PCI curve in Figure 2B has shown a single plateau pressure corresponding to the transition between the initial alloy to the final dihydride phase. To confirm this single step phase transition with hydrogen, we have performed *in-situ* neutron diffraction experiments during deuterium desorption by constant heating with 1 K/min under dynamic vacuum up to 713 K. Figure 6 displays the *in-situ* neutron diffractograms as a function of temperature (left) together with the vacuum pressure readings throughout the experiment (right).

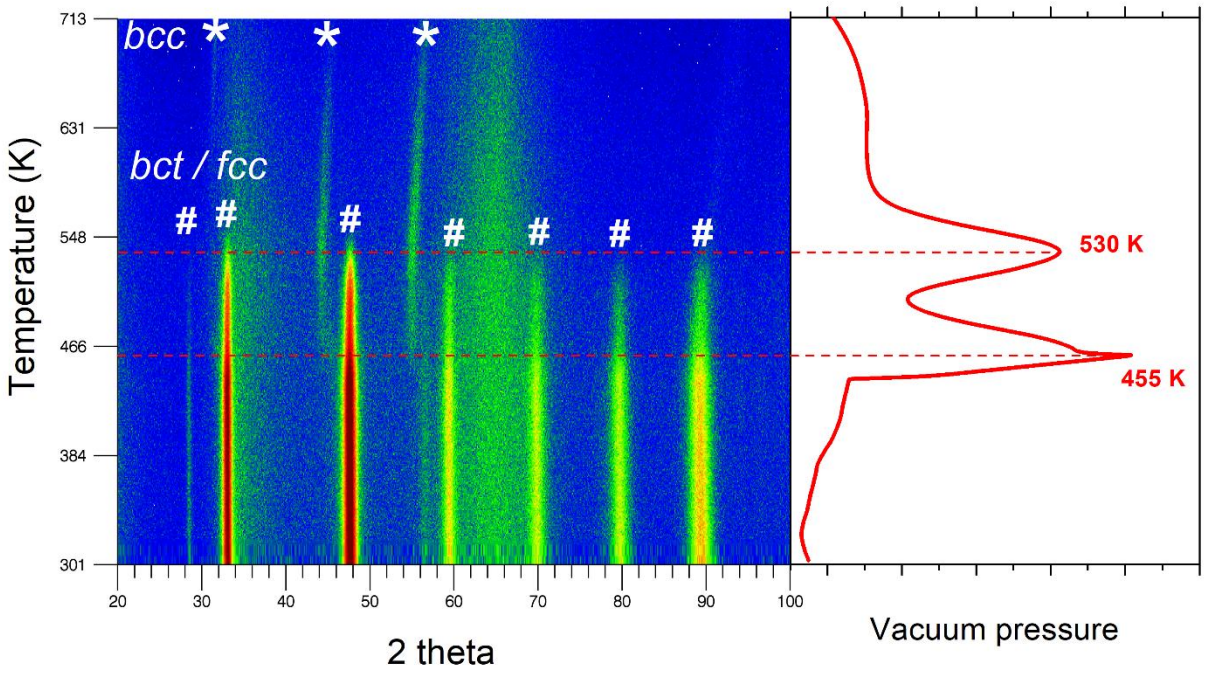

Figure 6. In-situ neutron diffraction of $Ti_{0.30}V_{0.25}Zr_{0.10}Nb_{0.25}Ta_{0.10}D_2$ (λ = 1.28 Å) during heating with 1 K/min up to 713 K (left) under dynamic vacuum and the corresponding gas desorption signal (right).

The diffraction peaks from the *bct/fcc* deuteride phase initially present are marked with hash symbols (#). The unmarked and broad peaks between 30 - 35 ° and 60 - 70 ° belong to the silica tube used as sample holder. From bottom-up, we observe that the deuteride remains stable from room temperature up to ~ 400 K. This temperature marks the beginning of the desorption process accompanied by a gradual decrease of the *bct/fcc* lattice peak's intensity. The strongest drop of *bct/fcc* peak's intensity arises at the maximum of the first desorption peak at around 455 K associated with the formation of a new *bcc* phase identified with star symbols (*). Between 455 and 530 K, the two phases coexist. A second desorption peak occurs at 530 K when the *bct/fcc* phase disappears and the deuteride completely transforms into a *bcc*

structure. Above 530 K, only the peaks from the *bcc* phase are visible and they gradually shift towards higher 2Θ angles while increasing temperature. This shift can be related to a lattice shrinkage due to deuterium atoms desorbing from the interstitial sites of the *bcc* phase, also confirmed by a broad feature in the gas desorption signal in this temperature region. A very good agreement is displayed between the phase transition noticed in the neutron thermo-diffractograms and the gas desorption peaks recorded during dynamic vacuum. The diffraction peaks of the desorbed alloy are very weak as compared to the deuteride phase due to its low thermal neutron cross-section. This peculiar feature makes this type of refractory MPEA with high melting point and high neutron transparency interesting candidates as cladding materials for nuclear reactors.[21]

From this *in situ* experiment, we conclude that the desorption from the deuteride phase induces a progressive single transformation from *bct/fcc* → *bcc*, as also demonstrated earlier for TiVZrNbHf [7,20], Ti-V-Zr-Nb [15] and Ti-Zr-Hf-Mo-Nd [13]. The observed *bcc* phase at high temperature is an interstitial solid solution with deuterium. The single step transition revealed here agrees with the PCI curve recorded at room temperature while, in contrast to conventional *bcc* alloys that usually have two transition steps (*bcc* ↔ *bct* ↔ *fcc*).[22,23]

It is worth to compare the *in situ* neutron diffraction patterns during deuterium desorption from the present quinary alloy with the quaternary composition $Ti_{0.325}V_{0.275}Zr_{0.125}Nb_{0.275}$, without Ta, prepared by the same technique (arc melting). The neutron diffraction thermo-diffractograms for the latter alloy recorded under similar conditions are shown in figure SI2. Interestingly, the desorption occurs in a single step with an abrupt phase transformation at around 540 K, without coexistence of the deuteride/alloy region. As observed, the phase

transformation in the quaternary alloy occurs at around 100 K higher temperature than in the quinary alloy containing Ta. Similarly to TDS findings, *in situ* neutron diffraction demonstrated that the quinary alloy possesses improved desorption properties relative to the quaternary alloy.

Therefore, the addition of only 10 % Ta into $Ti_{0.325}V_{0.275}Zr_{0.125}Nb_{0.275}$ not only increases the maximum capacity but also decreases the thermal stability of the hydride phase by around 100 K. It was recently proposed that the valence electron concentration (VEC) may play an important role for hydrogen desorption: the onset temperature for hydrogen desorption decreases linearly with VEC parameter.[12] Presently, VEC values are very similar since only elements from columns 4 and 5 of the periodic table are used (4.6 and 4.55 for $Ti_{0.30}V_{0.25}Zr_{0.10}Nb_{0.25}Ta_{0.10}$ and $Ti_{0.325}V_{0.275}Zr_{0.125}Nb_{0.275}$, respectively). Therefore, the use of VEC parameter to explain the change of the onset temperature is unlikely in our case. Moreover, the TDS, DSC and *in situ* neutron diffraction experiments are in full agreement showing two desorption peaks that result from intrinsic kinetics of the hydride/deuteride phase during desorption and not from two different phase transitions.

3.4 Hydrogen absorption/desorption cycling

The absorption/desorption reversibility and the structural stability of the MPEA were tested by measuring the hydrogen absorption capacity (at 298 K and 30 bar H_2 pressure) followed by desorption (dynamic vacuum at 673 K for 5 h) during 20 cycles (Figure 7). The maximum hydrogen uptake is observed for the first cycle with a capacity of 2.0 H/*M* (2.52 wt.%). After the first cycle, a smooth decrease in H_2 capacity occurs until a stabilization is reached at the 8th

cycle, where the alloy can reversibly store approximately 86 % of its initial capacity (1.71 H/*M*; 2.19 wt.%).

Interestingly, the kinetic of absorption is very fast reaching full capacity within 2-3 minutes and improves with cycling, as demonstrated for the first and tenth absorption cycles (Figure SI3).

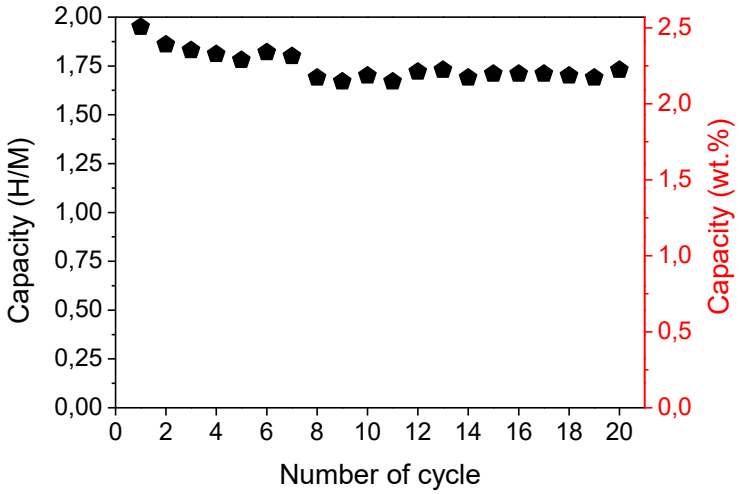

Figure 7. Hydrogen absorption capacity of $Ti_{0.30}V_{0.25}Zr_{0.10}Nb_{0.25}Ta_{0.10}$ upon hydrogen absorption/desorption cycling (20 cycles).

The slight decay of the hydrogen storage capacity during cycling is a common feature for the *bcc* alloys both classical and MPEA.[15] In order to better describe this behavior, a second DSC-QMS measurement was performed on the hydride phase after 10 absorption/desorption cycles. The initial DSC-QMS curve, described earlier, together with the measurement after 10 cycles are plotted in Figure 8. The QMS signals show a perfect correlation with the DSC endothermic signals, irrespective of cycle number.

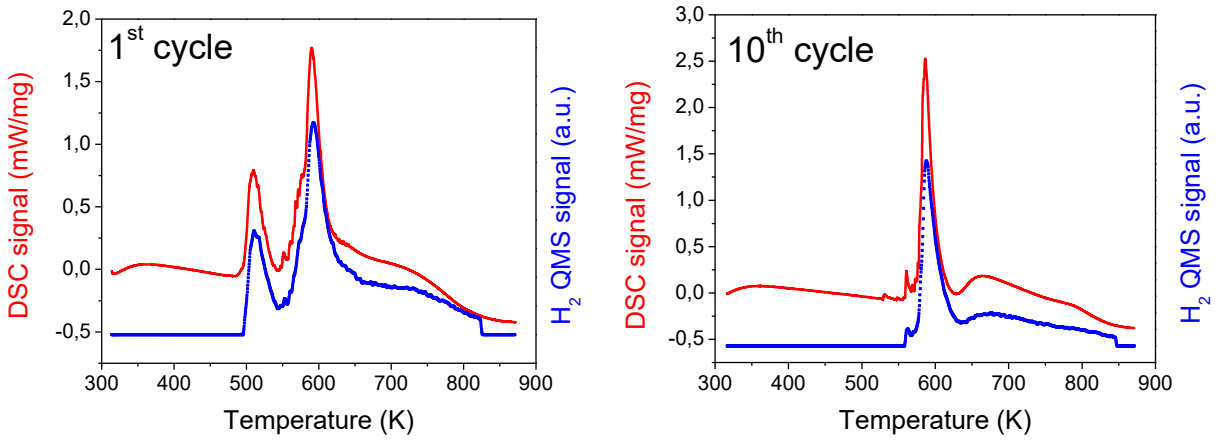

Figure 8. DSC-QMS curves for the first desorption (left) and tenth absorption/desorption cycles (right) upon a heating ramp of 10 K/min.

The cycled alloy (right plot in Figure 8) has a single endothermic event at around 590 K matching to the second desorption feature of the first DSC curve (left plot in Figure 8). This suggests that the absence of the first endothermic event for the cycled sample may be related to the capacity loss upon cycling. A simple comparison between the integrated area under the QMS signals for the first and tenth cycles informs us about this decrease. Thus, the area after 10 cycles is around 84 % of the initial one, in good agreement with the cycling results. Losing hydrogen capacity over cycling is a widespread phenomenon reported in many studies and sometimes explained by phase segregation. To check possible phase segregation, we have carried out SEM investigations after the first and twentieth cycle. The development of many cracks can be noticed after 20 cycles without any sign of phase segregation (Figure SI4). The DSC-QMS measurements in Figure 8 provides some new insights into this behavior; however, the reason for this capacity drop is still unclear since no phase segregation is noticed during cycling, as further confirmed by XRD.

In order to check the structural stability over cycling, the XRD patterns of the *bcc* and the *bct/fcc* hydride phases for the first and last cycle are compared in Figure 9. The desorbed alloy after 20 cycles recovers the initial *bcc* structure with a = 3.246(5) Å very close to the initial value a = 3.263(1) Å (Figure 9A). Similarly, the *bct/fcc* phase corresponding to the hydride after 20 cycles shows similar lattice parameters (*bct* lattice: a = 3.157(1) Å and c = 4.491(2) Å or *fcc* lattice: a = 4.474(1) Å) as the material after the first hydrogen absorption (*bct* lattice: a = 3.155(3) Å and c = 4.515(3) Å or *fcc* lattice: a = 4.482(6) Å). The major change is related to peak broadening noticed for both *bcc* and *bct/fcc* phases after 20 cycles. However, this is not surprising since extensive hydrogen absorption/desorption is well known to refine the grains and to increase the defects and the strain within the materials. We hypothesize that the loss of crystallinity upon cycling might be responsible for the decrease of capacity. In order to support this hypothesis, we have employed mechanochemical methods for the preparation of the same initial alloy and related hydride, further discussed in the next section. A simple comparison of the performances of all these materials seems to suggest that alloys with reduced crystallinity, typically synthesized by ball milling, have inferior hydrogen absorption capacity than highly crystalline alloys, as obtained by classical high-temperature fusion methods. Furthermore, recently, it was proven that the size and the concentration of vacancy clusters in Ti-Zr-Nb-Ta MPEA significantly increases after activation as compared to pure Nb metal.[24]

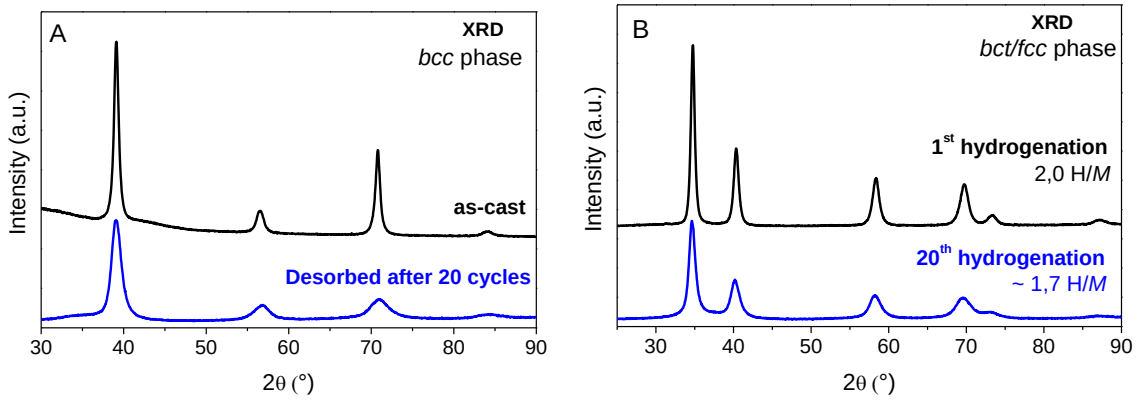

Figure 9. XRD patterns of $Ti_{0.30}V_{0.25}Zr_{0.10}Nb_{0.25}Ta_{0.10}$ before and after 20 cycles as initial and desorbed phases (A) and hydride phases (B) for the 1st and 20th cycles.

In summary, despite around 14% loss of capacity after 20 cycles, the crystalline structures of the $Ti_{0.30}V_{0.25}Zr_{0.10}Nb_{0.25}Ta_{0.10}$ alloy/hydride are preserved without any obvious phase segregation or oxidation, as previously reported in several refractory MPEAs.[24] The loss noticed for the quinary alloy, 14%, is smaller than 26% capacity drop recorded for the quaternary alloy during cycling.[15] One possible explanation might be the preparation method: the quaternary hydride was prepared by reactive ball milling (high energy ball milling under high H_2 pressure), whereas the present alloy was synthesized by arc-melting. The ball milling material is very sensitive to oxidation; on the contrary, the arc-melting alloy in the form of coarse powder might be less prone to oxidation and thus better preserving the cycling performances.

This alloy has demonstrated to withstand cycling with superior hydrogen capacity (~ 2.2 wt.%) and reversibility than other *bcc* refractory MPEAs: Ti-V-Zr-Nb [15] and TiVCrNb [12].

3.5 Other synthetic methods

Recently, we have reported that MPEAs can be also prepared by mechanochemical methods in both alloy and hydride forms.[15] In a very similar way, we have presently employed these techniques and successfully prepared single-phase initial *bcc* alloy by high energy ball milling under inert atmosphere as well as single-phase hydride by high energy ball milling under hydrogen pressure. The main aim here is to compare the hydrogen absorption performances of the ball-milled materials with the alloy obtained by high-temperature fusion method. All synthetic details together with structural and hydrogen sorption characterizations are given in SI.

XRD performed on the ball-milled alloy together with neutron diffraction experiments on the deuteride phase confirm broad diffraction peaks which suggests materials with small crystallite sizes and reduced degree of crystallinity. The ball-milled *bcc* alloy can absorb hydrogen at relatively high temperature (around 400 K) forming a hydride phase with 1.8 H/*M* capacity (2.3 wt.%), as detailed in SI. Moreover, our previous findings on the quaternary system also confirmed that materials prepared by ball milling under inert gas have the slowest absorption kinetics and the smaller capacity than the alloys obtained by the other synthetic methods [15].

The reactive ball milling under hydrogen atmosphere directly produces a single-phase hydride material with 1.7 H/*M* capacity (2.2 wt.%) after 1 h of process. As expected, the hydride phase adopts a *bct/fcc* lattice and it is characterized by small crystallite sizes and reduced degree of crystallinity (see SI).

Lastly, these findings suggest that the material crystallinity might be responsible for the loss of capacity in the present MPEA. Materials with a large number of deformations and defects, as produced by ball milling, have demonstrated poorer hydrogen storage performances when compared to the same material with a high degree of crystallinity, as commonly prepared by high-temperature fusion techniques. Regardless, the ball milling method is still a good alternative to prepare MPEAs and related hydrides containing metals with low melting temperatures and high vapor pressure.

4. Conclusions

The MPEA with the composition $Ti_{0.30}V_{0.25}Zr_{0.10}Nb_{0.25}Ta_{0.10}$ was prepared by classical arc-melting technique adopting a single-phase *bcc* lattice. The alloy absorbs a large amount of hydrogen at room temperature up to 2.0 H/*M* forming a *bct/fcc* lattice where hydrogen occupies the tetrahedral interstitial sites. As proven by the PCI and neutron diffraction experiments, the hydrogenation of the alloy occurs in a singlephase transformation from *bcc* ↔ *bct/fcc*. As compared with the quaternary alloy $Ti_{0.325}V_{0.275}Zr_{0.125}Nb_{0.275}$ the addition of 10 % of Ta improves significantly the hydrogen capacity, the desorption properties and the stability during cycling.

Acknowledgment

We acknowledge ILL for beamtime allocation on the CRG-D1B beamline. Fabrice Couturas from ICMPE and Sofien Djellit, technician on D1B, are acknowledged for help with neutron diffraction at ILL. Valerie Lalanne from ICMPE and Flavio Jose Antiqueira from UFSCAR are thanked for precious help with arc melting and calorimetry measurements, respectively. Fermin Cuevas from ICMPE is thanked for help with analysis of data by reactive ball milling. The authors

acknowledge the French National Research Agency (ANR) for the financial support for the MASSHY project (ANR-19-CE05-0029-01) and CAMPUS France for financial support within the exchange French-Bresilan COFECUB-CAPES program. MS and GE acknowledge financial support from the NordForsk Nordic Neutron Science Programme through the Functional hydrides (FunHy) project (grant number 81942).

References:

[1] A.M. Abdalla, S. Hossain, O.B. Nisfindy, A.T. Azad, M. Dawood, A.K. Azad, Hydrogen production, storage, transportation and key challenges with applications: A review, Energy Convers. Manag. 165 (2018) 602–627. https://doi.org/10.1016/j.enconman.2018.03.088.

[2] J.-C. Crivello, B. Dam, R.V. Denys, M. Dornheim, D.M. Grant, J. Huot, T.R. Jensen, P. de Jongh, M. Latroche, C. Milanese, D. Milcius, G.S. Walker, C.J. Webb, C. Zlotea, V.A. Yartys, Review of magnesium hydride-based materials: development and optimisation, Appl. Phys. -Mater. Sci. Process. 122 (2016).

[3] D.B. Miracle, O.N. Senkov, A critical review of high entropy alloys and related concepts, Acta Mater. 122 (2017) 448–511. https://doi.org/10.1016/j.actamat.2016.08.081.

[4] M.C. Gao, D.B. Miracle, D. Maurice, X. Yan, Y. Zhang, J.A. Hawk, High-entropy functional materials, J. Mater. Res. (2018) 1–18. https://doi.org/10.1557/jmr.2018.323.

[5] D.B. Miracle, High entropy alloys as a bold step forward in alloy development, Nat. Commun. 10 (2019) 1805. https://doi.org/10.1038/s41467-019-09700-1.

[6] I. Kunce, M. Polanski, J. Bystrzycki, Microstructure and hydrogen storage properties of a TiZrNbMoV high entropy alloy synthesized using Laser Engineered Net Shaping (LENS), Int. J. Hydrog. Energy. 39 (2014) 9904–9910. http://dx.doi.org/10.1016/j.ijhydene.2014.02.067.

[7] M. Sahlberg, D. Karlsson, C. Zlotea, U. Jansson, Superior hydrogen storage in high entropy alloys, Sci. Rep. 6 (2016). https://doi.org/10.1038/srep36770.

[8] G. Zepon, D.R. Leiva, R.B. Strozi, A. Bedoch, S.J.A. Figueroa, T.T. Ishikawa, W.J. Botta, Hydrogen-induced phase transition of MgZrTiFe0.5Co0.5Ni0.5 high entropy alloy, Int. J. Hydrog. Energy. 43 (2018) 1702–1708. https://doi.org/10.1016/j.ijhydene.2017.11.106.

[9] H. Shen, J. Zhang, J. Hu, J. Zhang, Y. Mao, H. Xiao, X. Zhou, X. Zu, A Novel TiZrHfMoNb High-Entropy Alloy for Solar Thermal Energy Storage, Nanomaterials. 9 (2019) 248. https://doi.org/10.3390/nano9020248.

[10] C. Zlotea, M.A. Sow, G. Ek, J.-P. Couzinié, L. Perrière, I. Guillot, J. Bourgon, K.T. Møller, T.R. Jensen, E. Akiba, M. Sahlberg, Hydrogen sorption in TiZrNbHfTa high entropy alloy, J. Alloys Compd. 775 (2019) 667–674. https://doi.org/10.1016/j.jallcom.2018.10.108.

[11] M.M. Nygård, G. Ek, D. Karlsson, M. Sahlberg, M.H. Sørby, B.C. Hauback, Hydrogen storage in high-entropy alloys with varying degree of local lattice strain, Int. J. Hydrog. Energy. 44 (2019) 29140–29149. https://doi.org/10.1016/j.ijhydene.2019.03.223.

[12] M.M. Nygård, G. Ek, D. Karlsson, M.H. Sørby, M. Sahlberg, B.C. Hauback, Counting electrons - A new approach to tailor the hydrogen sorption properties of high-entropy alloys, Acta Mater. 175 (2019) 121–129. https://doi.org/10.1016/j.actamat.2019.06.002.

[13] H. Shen, J. Hu, P. Li, G. Huang, J. Zhang, J. Zhang, Y. Mao, H. Xiao, X. Zhou, X. Zu, X. Long, S. Peng, Compositional dependence of hydrogenation performance of Ti-Zr-Hf-Mo-Nb high-entropy alloys for hydrogen/tritium storage, J. Mater. Sci. Technol. (2020). https://doi.org/10.1016/j.jmst.2019.08.060.

[14] Y. Fukai, The Metal-Hydrogen System, Springer-Verlag, Berlin/Heidelberg, 2005.

[15] J. Montero, C. Zlotea, G. Ek, J.-C. Crivello, L. Laversenne, M. Sahlberg, TiVZrNb Multi-Principal-Element Alloy: Synthesis Optimization, Structural, and Hydrogen Sorption Properties, Molecules. 24 (2019) 2799. https://doi.org/10.3390/molecules24152799.

[16] J. RODRIGUEZCARVAJAL, RECENT ADVANCES IN MAGNETIC-STRUCTURE DETERMINATION BY NEUTRON POWDER DIFFRACTION, Phys. B. 192 (1993) 55–69. https://doi.org/10.1016/0921-4526(93)90108-I.
[17] C. Zlotea, C. Chevalier-César, E. Léonel, E. Leroy, F. Cuevas, P. Dibandjo, C. Vix-Guterl, T. Martens, M. Latroche, Synthesis of small metallic Mg-based nanoparticles confined in porous carbon materials for hydrogen sorption, Faraday Discuss. 151 (2011) 117–131.
[18] Y.F. Ye, Q. Wang, J. Lu, C.T. Liu, Y. Yang, High-entropy alloy: challenges and prospects, Mater. Today. 19 (2016) 349–362. https://doi.org/10.1016/j.mattod.2015.11.026.
[19] Gordon Aylward, Tristan Findlay, SI Chemical Data, 3rd edition, J. Chem. Educ. 72 (1995) A109. https://doi.org/10.1021/ed072pA109.1.
[20] D. Karlsson, G. Ek, J. Cedervall, C. Zlotea, K.T. Møller, T.C. Hansen, J. Bednarčík, M. Paskevicius, M.H. Sørby, T.R. Jensen, U. Jansson, M. Sahlberg, Structure and Hydrogenation Properties of a HfNbTiVZr High-Entropy Alloy, Inorg. Chem. 57 (2018) 2103–2110. https://doi.org/10.1021/acs.inorgchem.7b03004.
[21] D.J.M. King, S.T.Y. Cheung, S.A. Humphry-Baker, C. Parkin, A. Couet, M.B. Cortie, G.R. Lumpkin, S.C. Middleburgh, A.J. Knowles, High temperature, low neutron cross-section high-entropy alloys in the Nb-Ti-V-Zr system, Acta Mater. 166 (2019) 435–446. https://doi.org/10.1016/j.actamat.2019.01.006.
[22] Y. Nakamura, K. Oikawa, T. Kamiyama, E. Akiba, Crystal structure of two hydrides formed from a Ti–V–Mn BCC solid solution alloy studied by time-of-flight neutron powder diffraction — a NaCl structure and a CaF2 structure, J. Alloys Compd. 316 (2001) 284–289. https://doi.org/10.1016/S0925-8388(00)01503-6.
[23] K. Sakaki, H. Kim, K. Asano, Y. Nakamura, Hydrogen storage properties of Nb-based solid solution alloys with a BCC structure, J. Alloys Compd. 820 (2020) 153399. https://doi.org/10.1016/j.jallcom.2019.153399.
[24] C. Zhang, Y. Wu, L. You, X. Cao, Z. Lu, X. Song, Investigation on the activation mechanism of hydrogen absorption in TiZrNbTa high entropy alloy, J. Alloys Compd. 781 (2019) 613–620. https://doi.org/10.1016/j.jallcom.2018.12.120.